

**PAPER 143**  
**HELICOPTER EMERGENCY MEDICAL SERVICE (HEMS) FROM A ROOFTOP IN  
 AMSTERDAM: A SIMULATION PERSPECTIVE**

by

**Henk Haverdings**

National Aerospace Laboratory NLR

Amsterdam, The Netherlands

e-mail: [haverdi@nlr.nl](mailto:haverdi@nlr.nl)

**ABSTRACT**

For helicopter emergency medical operations from an Amsterdam hospital roof top the airflow for 2 wind conditions was computed using 2 CFD applications of a flow solver, viz. the RANS solver and the hybrid RANS-LES solver. From the generated data both the detailed mean wind flow around the building as well as the random-varying turbulent fluctuations were derived and implemented in a real-time simulation. Pilots, experienced with the actual wind climate around the building found the realism quite acceptable, even though a fixed-base simulator was used. The wind and turbulence modelling approach was very acceptable in terms of accuracy and effort to implement in a simulator. Future applications of the same modelling approach can be the wind flow modelling around oil rigs and around ships in case of helicopter-ship operations.

**NOMENCLATURE**

ACP	Aerodynamic Computation Point
ANWB	General Dutch Automobile Association (in Dutch)
CFD	Computational Fluid Dynamics
EARSM	Explicit Algebraic Reynolds Stress Model
GRC	Green RotorCraft
$H_u$	Transfer function in $u$ -component of turbulence
HEMS	Helicopter Emergency Medical Service
HPS	Helicopter Pilot Station
$k$	Turbulent kinetic energy
LES	Large-Eddy Simulation
$L_u, L_v, L_w$	Turbulent scale lengths (Dryden turbulence)
$\ell$	Turbulent scale length in CFD models
MAA	Medical Air Assistance
NLR	National Aerospace Laboratory The Netherlands
NVG	Night Vision Goggle
RANS	Reynolds-Averaged Navier-Stokes
RNLAF	Royal Netherlands Air Force
$T$	averaging time interval
$T_u, T_v, T_w$	(Dryden) filter time constants
$U, V, W$	Wind components in x, y and z direction
$u, v, w$	Turbulence components in x, y and z direction
$V_{wind}$	Windspeed
VFR	Visual Flight Rules
VU	Free University (in Dutch)
$z_0$	Roughness length
$\Delta t$	Time step in numerical computations
$\epsilon$	Eddy dissipation rate
$\sigma$	Standard deviation
$\omega$	Specific dissipation rate

## 1 INTRODUCTION

Close to NLR in Amsterdam, The Netherlands, a Helicopter Emergency Medical Service (HEMS) is provided from a helideck on the roof of the nearby 'VU' = "Vrije Universiteit" (Free

University) university hospital. Basically day-VFR operations are carried out, but since February 2011 night-VFR operations are also carried out using NVGs. No means yet existed to support this type of operations using real-time helicopter simulation. To provide this support,

as well as to expand the helicopter simulation facility capability of NLR the wind climate around the VUmc hospital was modelled by performing CFD calculations using



first a Reynolds-Averaged Navier-Stokes solver (RANS), in conjunction with a closed-form turbulence model called  $k-\omega$  EARSM: the  $k-\omega$  two-equation turbulence model enhanced with an Explicit Algebraic Reynolds Stress Model. The steady-state wind flow around the building complex as well as the closed-form turbulence characteristics (turbulent kinetic energy, eddy dissipation) were determined for a structured grid of  $7.1 \cdot 10^6$  points forming  $6.4 \cdot 10^6$  cells, spanning a space of 677 m long, 627 m wide and 350 m high. Rather than solving the time-varying airflow situation around the building using a time-consuming, complex Large Eddy Simulation (LES) it was decided to first use the RANS to find a steady-state flow solution together with the unknown parameters of the turbulence model.

As a later application a hybrid RANS-LES computation was performed, where the RANS was used to set up the boundary layer and the LES was used to compute the time-varying development of the complete flow around the building. Once the initial transients had disappeared, time averages were taken of the flow components to both compute mean flow as well as the standard deviations, which are a measure of the flow variability, akin to turbulence. This is a first attempt at NLR to model complex flows around bluff bodies, and to make it suitable for real-time use in a simulator.

## 2 HEMS OPERATIONS IN THE NETHERLANDS

### 2.1 Operating principles, concept and mission

The ANWB Medical Air Assistance (MAA) operates the medical helicopters. It is a Dutch Helicopter operator with a socially supportive task. Under contract with medical health insurance companies and hospitals on a national

scale it serves, among others, 4 trauma centres distributed all over The Netherlands.

The MAA is an independent subsidiary of the Royal Dutch Automobile Association 'ANWB', operating 4 helicopters from the 4 trauma centres at the moment. With 4 helicopters on station, with 2 in reserve, it covers the entire Netherlands. Each such "trauma" helicopter is nick-named "Life-liner", a name also used in the radio R/T call-sign ("Life-liner 1" to "Life-liner 4"). On May 1<sup>st</sup>, 1995, in cooperation with the Free University ('VU') hospital in Amsterdam, The Netherlands, the MAA started to post "trauma helicopters" at the VUmc<sup>1</sup> hospital. Since then about 33,000 flights have been made. At the moment the MAA is an organization employing 36 people, and making more than 4,200 flights per year.



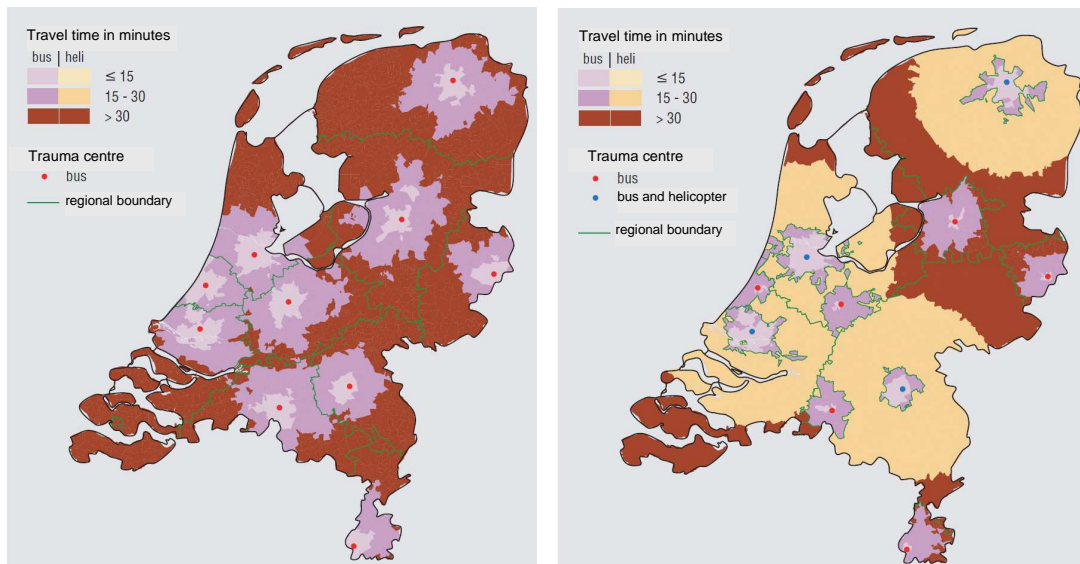
**Figure 1 MAA helicopter "Life-liner 1" in action on the Dam Square in Amsterdam**

Contrary perhaps to the functioning of medevac flights in other countries it is not a question of "first come, first serve" that determines which medevac helicopter takes the medical case / patient. A regional Reporting & Dispatch Unit receives the emergency call, and it determines, based on the information received if, and if so, which Life-liner(s) is to be dispatched to the accident scene. This choice depends on the requirement that medical aid should be available at the accident site within 30 minutes.

The purpose of the helicopter is to bring in a "trauma surgeon", who in principle will stay with the victim/patient and will go with him/her to the nearest hospital in the ambulance that has also been dispatched to the same scene<sup>2</sup>. Especially patients who have been intubated should not be transferred from litter to litter and

<sup>1</sup> The additive 'mc' stands for "medical centre", as the VU owns more buildings.

<sup>2</sup> The ambulances do not carry personnel qualified to perform such traumatic actions like surgery.



a) Night-time travel time, without helicopters

b) night-time travel time with 4 helicopters

**Figure 2** Travel time distribution in the Netherlands, with or without helicopters (from Ref. [1])

might therefore have to be transported by air. Depending upon the judgment of the surgeon on the patient's condition and on local traffic or other conditions the surgeon might decide to take the patient on board the helicopter for a flight back to the nearest hospital suitable to take helicopters. Four such hospitals are available in the Netherlands, viz. Amsterdam (VU medical centre), Rotterdam (Erasmus hospital) Groningen and Nijmegen (Radboud hospital). The pilots are mostly recruited from the RNLAf, and most, if not all of them, have had previous (military) exposure to the use of night vision goggles (NVGs). A one-year trial period

vicinity of a helicopter-equipped hospital the bus has a shorter travel time than the helicopter.

### 3 VUMc BUILDING ROOFTOP HELIPAD

#### 3.1 Location/site survey

The building is quite a complex with several wings and other high-rise buildings, existing or under construction, nearby. The VUmc building size is roughly 77 m long by 24 m wide by 40 m high.

**Figure 3** Views of the VUmc hospital building & rooftop (encircled in red)

was held, starting November 2006, to evaluate the suitability of night operations, making use of NVGs to avoid obstacles such as power lines (Ref. [1]).

As Figure 2 shows the (computed) time to reach any accident site, the "travel time", is reduced considerably when using 4 medevac helicopters at night, compared to the same condition using only a medical bus (ambulance). Note that for Nijmegen Radboud hospital the medevac helicopter was stationed at the nearby military airbase Volkel. Note also that in the immediate

For the CFD computations a computational domain structured grid was defined, spanning a space of 624 x 620 x 60 m containing the VUmc building. The VUmc building height levels are shown in Figure 4. The CFD grid is actually much finer than shown in this figure.

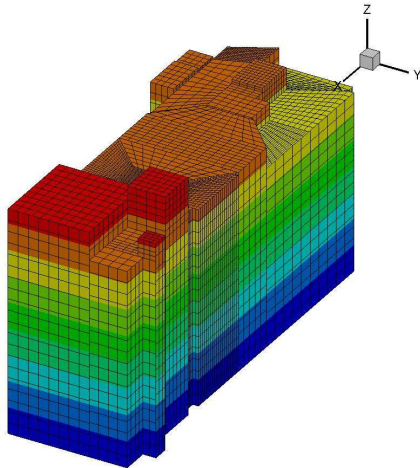


**Figure 4** VUmc building geometric grid (colours indicate height)

Near the flight deck the grid was refined to cells having a size less than 1x1x1 m.

## 3.2 Wind flow calculations

### 3.2.1 General

The computation of the wind flow over the VUmc building could be solved in various ways. The “simplest” one is to use the RANS solver, or Reynolds-Averaged Navier-Stokes solver. This solver is coupled to a turbulence model, for which NLR selected the  $k-\omega$  EARSM model (Explicit Averaged Reynolds Stress Model), see e.g. Refs. [2] and [3]. A boundary layer velocity profile involving the roughness length  $z_0$  (see [4]) is used to describe the lower atmospheric boundary layer at the inflow boundaries. The flow solver, together with the prescribed boundary conditions, solves the wind flow in the domain of interest, including any objects, assuming the flow can be described by a steady-state condition. The parameters selected for further processing are the 3 mean velocity components  $\bar{U}(x, y, z)$ ,  $\bar{V}(x, y, z)$  and  $\bar{W}(x, y, z)$ , the turbulent kinetic energy  $k(x, y, z)$ , the eddy dissipation rate  $\epsilon(x, y, z)$ , and many other parameters. The basic assumption is that the flow has reached steady-state.

The next level of complexity, with more leeway as to assumptions made, is to apply the hybrid RANS-LES solver. In addition to RANS a Large Eddy Simulation LES is applied. The RANS runs the closed-form  $k-\omega$  EARSM turbulence model for the boundary layer build-up, while the LES describes the time-varying flow pattern outside of wall layers as function of time. After a certain time interval, when the start-up process is assumed to have quieted down, the solver also

starts computing mean values and standard deviations of the wind flow components, which can be used later-on in various applications. The variance (standard deviation squared) of the wind components are a measure of the turbulent kinetic energy and should not differ “too much” from the RANS solution. If it does then very likely the assumption of steady-state, used with RANS, may not be applicable. With bluff bodies such as buildings, where large areas of separated flow may exist, the steady-state condition may well be questionable.

### 3.2.2 CFD solver

For the first application of solving the wind flow the RANS solver was applied, in conjunction with the  $k-\omega$  EARSM turbulence model. Later-on it was decided to also use the hybrid RANS-LES solver, where the RANS is used to build up the lowest part of the boundary layer, and to let the LES do the simulation in the time domain of the wind flow characteristics. More details can be found in Refs. [5] to [8].

To model the flow a structured grid was composed in a domain around the VUmc building of from -364 m to +313 m long, from -328 m to +300 m wide, and from the ground (0 m) to +350 m high. Total number of grid points amounted to  $7.1 \cdot 10^6$ . Near the building and the heli deck the cell size was reduced in order to have a higher-accuracy modelling of the flow.

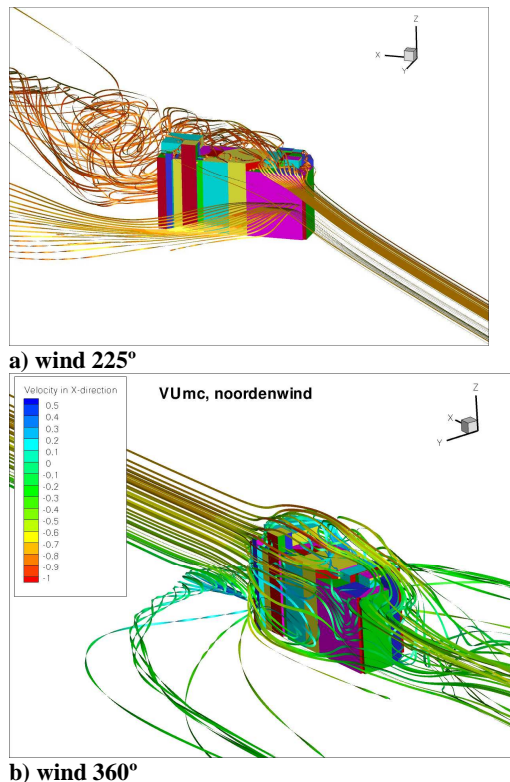
To model the effect of the environment a proper value of roughness length  $z_0$  (see Ref. [4]) was selected for the atmospheric boundary layer, which acted as the inflow boundary condition.

Initial values for turbulent kinetic energy were set close to zero, and the flow was solved for a wind speed of 20 Kt, for 2 wind conditions, viz. 225° and 360°.

The computations were performed on a FASET super-computer having 64 nodes, with 8 parallel processors per node. Total calculation time for the hybrid RANS-LES is estimated at 4000 h cpu time.

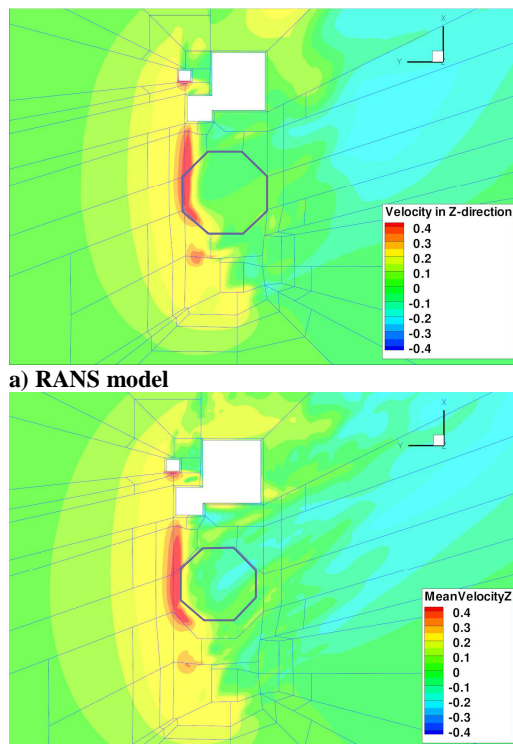
### 3.2.3 Mean wind flow for 2 wind directions

The resulting airflow has so far been calculated for 2 conditions, viz. the nominal wind direction of 225° and a windspeed of 20 Kt, and for the 360° wind direction, also at 20 Kt. From private information it is known that the calculated results for 225° agreed well with measured wind tunnel data.



a) wind 225°  
 b) wind 360°  
**Figure 5 Mean wind flow streams (ribbons) for the RANS wind model**

For the 225° case (Figure 5a) the air flow downwind of the building has become quite



a) RANS model  
 b) RANS-LES wind model  
**Figure 6 Mean vertical wind component for the RANS and RANS-LES wind model. Wind 225°**

messy, as expected. Note that the ribbons, or streamlines, show the mean direction of the flow, at different speeds (colouring scheme along the ribbon varies with speed).

For the 360° case (Figure 5b) one can see a ground vortex form just upwind of the building. Besides the mean flow components also (steady-state) turbulence exists, see the next chapter.

More importantly perhaps is the evolution of the vertical wind component, as it drives the power requirement to maintain (near) hovering flight. It is furthermore interesting to see the difference between the RANS and the RANS-LES wind model. In Figure 6 the vertical wind component is shown for a wind from 225° for the two wind models. Differences look small, fortunately.

## 4 TURBULENCE MODELING

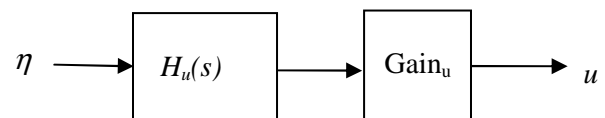
In the simulation of wind around a building turbulence is an important contributor to pilot workload. This turbulence is generated by the wake of the airflow around the building.

The turbulence intensity comes from the flow computations with the Reynolds-Average Navier-Stokes (RANS) solver, in conjunction with the turbulence model, of which many varieties exist. NLR uses the so-called  $k-\omega$  EARSM (Explicit Algebraic Reynolds Stress Model) turbulence model, from which turbulence quantities can be derived, see further on in sections 4.2 and 4.3.

To generate a real-time application of the turbulence, with proper spectral contents, 2 ways were applied, viz. 1) the Dryden model and 2a) the RANS or 2b) the hybrid RANS-LES model. The 3<sup>d</sup> way was no turbulence as a reference case. The 2 methods will be discussed next.

### 4.1 General modelling features

In order to be able to model or simulate turbulence, a white noise band-limited random signal  $\eta$  with unit variance is driven through colouring filters, or low-pass filters, the outputs of which is the sought-after turbulence, see the scheme below for the longitudinal component  $u$ :



Two basic parameters are needed to do this properly, viz. the time constant  $T_u$  of this first-order filter  $H_u$  and the turbulence intensity of the output of this filter  $\sigma_u$ . For the longitudinal component the low-pass filter is:

$$H_u = \frac{1}{T_u s + 1}$$

For the lateral and vertical gust component similar equations can be derived (Ref. [9]).

The turbulence intensity, described by the parameter  $\sigma_u$ , is obtained from the steady-state turbulent kinetic energy  $k$ , which is output by the RANS solver. In case of the hybrid RANS-LES solver it is obtained from the standard deviations of the flow quantities, which are computed at the end of the time series solution. Note that after the transfer function there is a gain block with a gain value

$$\text{Gain}_u = \sigma_u \sqrt{\frac{2T_u}{\pi} \cdot \frac{\pi}{\Delta t}} = \sigma_u \sqrt{\frac{2T_u}{\Delta t}}$$

The longer the time constant  $T_u$  the larger the gain, and vice-versa.

The time constants  $T_u$ ,  $T_v$  and  $T_w$  are obtained in two ways, viz. 1) by using the Dryden spectrum or 2) by using the eddy dissipation rate  $\epsilon$  computed by the CFD solver, in combination with the turbulent kinetic energy  $k$ , see sections 4.3.1 and 4.3.2 respectively.

## 4.2 Turbulence intensity

### 4.2.1 Dryden model turbulence intensity

For normal atmospheric applications the “rule of thumb” to find the turbulence intensity is that it relates to the wind speed by the rule (e.g. Ref. [9]):

$$\sigma_u = 0.1V_w$$

$$\frac{\sigma_v}{\sigma_u} = \frac{\sigma_w}{\sigma_u} = \frac{1}{(0.177 + 0.000623h)^{0.4}} \quad (1)$$

In this case of the VUmc building the turbulence intensity is obtained from the turbulent kinetic energy  $k$ , which is solved by the RANS flow solver, see the next sub-section.

### 4.2.2 RANS wind model turbulence intensity

In modelling the turbulent flow around a building, the closed-form turbulence in the RANS solver is solved using the so-called  $k - \omega$  EARSM turbulence model. Here  $k$  is the turbulent kinetic energy

$$k = \frac{1}{2} (\sigma_u^2 + \sigma_v^2 + \sigma_w^2) \quad (2)$$

where  $\sigma$  is the standard deviation of the Gaussian zero-mean turbulence components  $u$ ,  $v$  and  $w$  in  $x$ ,  $y$  and  $z$  direction respectively.

To obtain an estimate of the size of the individual turbulence intensity components one can apply Eq.(2) in reverse, leading to:

$$\sigma_u^2 + \sigma_v^2 + \sigma_w^2 = 2k$$

When assuming an equal share of kinetic energy among the 3 axes, then one can find:

$$\sigma_{u,v,w} = \sqrt{\frac{2}{3}}k \quad (3)$$

The turbulent kinetic energy  $k$  has been computed for the entire computational domain. The altitude of a level plane going through the rotor hub when on the deck (including skid height), is 2.95 m above the helipad or 41.66 m above the ground, The contours of  $k$  for an altitude of 45 m are shown for the 225° wind direction in Figure 7.

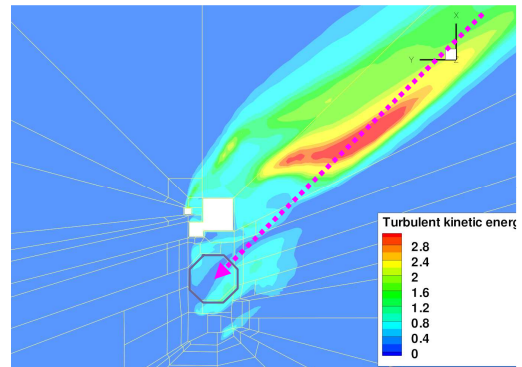
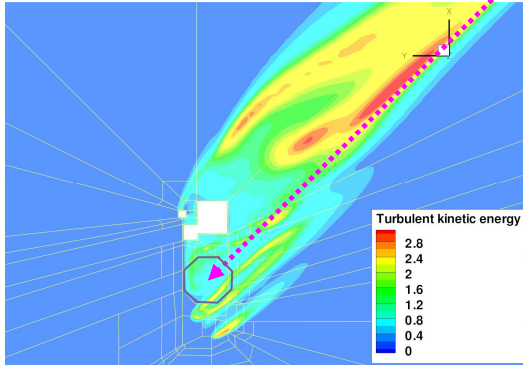


Figure 7 Turbulent kinetic energy  $k$  at 45m MSL. Wind direction 225°

The white area represents the (cut through the) VUmc building. The magenta line indicates a flight path course towards the helipad of 225° (into the wind), which would go just through or above the most intense turbulence area. It is apparent that there is some sort of cliff-edge or a ridge situation: there is no turbulence just to the left and the right of the line indicated above; Most of the wake of the building is to the right of the flight path. There is a strong gradient on the one side, but on the other side there is a more gradual variation in  $k$ . Largest value for  $k$  is  $3 \text{ m}^2/\text{s}^2$ , meaning that  $\sigma = \sqrt{\frac{2}{3}}k = \sqrt{2} = 1.4 \text{ m/s}$  (4.6 ft/s), or about 0.14 times the windspeed (20 KT = 10 m/s). This is a bit more than for the “standard” turbulence intensity value of 0.1 times the windspeed. The CAA (Ref. [10]) states a general heli deck operating limit on the turbulence of  $\sigma < 1.75 \text{ m/s}$  so in the above case, with a value of  $\sigma = 1.4 \text{ m/s}$ , there is no operational limit exceeded.

In the above turbulent flow the initial boundary condition values of  $k$  from where the air flow starts, i.e. the south and west boundaries, were set to zero, based on the assumption that there is

no mechanism that drives the turbulence, i.e. there will be only dissipation of kinetic energy down to a low level. However, when putting an initial boundary value of  $k=1 \text{ m}^2/\text{s}^2$  on the south and west boundaries, on the premise that there is some atmospheric turbulence of roughly  $\sigma=0.1V_{wind}$ , the steady-state solution becomes as depicted in Figure 8.



**Figure 8** Distribution of turbulent kinetic energy  $k$  at 45m MSL with non-zero boundary conditions; wind dir. 225°

Clearly an extra region with turbulent kinetic energy levels of about  $3 \text{ m}^2/\text{s}^2$  appears next to the first one already depicted in the previous figure. Also at the south and west boundaries some low values of  $k$  appear, but quickly dissipate. The intended flight path just rides along the high(er)-turbulence area, the same ridge situation as before. But overall the introduction of a non-zero boundary condition on  $k$  has had the effect of increasing the turbulent kinetic energy levels in the wake downwind of the building, where in fact most of the turbulence is generated. This result calls for caution when solving such a complex flow situation using a steady-state solution. A practical flying solution would be to approach the building in this case with a small crosswind of about 20°, i.e. a final track of 245° to clear the turbulent area.

In Figure 9 the same turbulent kinetic energy is shown for the wind from the north, i.e. a wind direction of 360°.

Pilots reported this condition to be more demanding. As one can see there is an area of turbulence both just before reaching the heli deck and to the left of the heli deck. In this case the flight path passes right through or above the wake coming off the building. From the maximum value of  $k = 4.6 \text{ m}^2/\text{s}^2$  one can derive a standard deviation, as previously done, of 1.75 m/s, i.e. it is just on the CAA-posed operational limit, provided the flight proceeds right through this area. A vertical profile along the approach direction shows the vertical development of  $k$  in Figure 10. It is clear that the

approach would bring the rotorcraft right

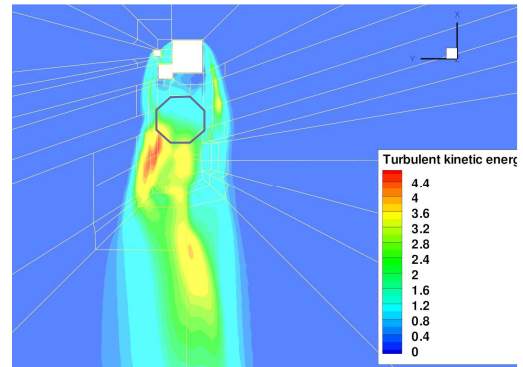


**Figure 9** Turbulent kinetic energy  $k$  for a wind direction of 360°

alongside, or even through, the high-turbulent area.

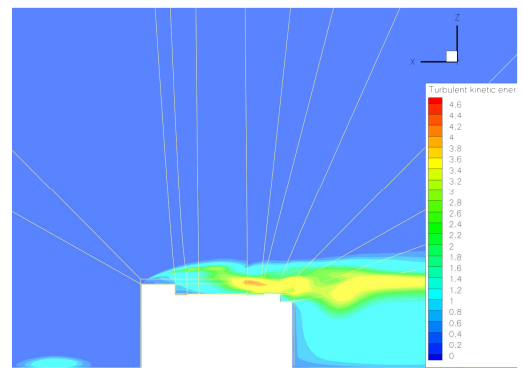


**Figure 10** Profile plot of turbulent kinetic energy for wind dir. of 360°

#### 4.2.3 Turbulence intensity with the RANS-LES wind model

In case of the hybrid RANS-LES wind field flow solver, after an assumed steady-state condition has been reached a mean flow and standard deviation (variance) is computed of the 3 flow components (among others) over a time averaging interval  $T$ . This results in the turbulence intensity component  $\sigma_u$  at the  $ijk^{\text{th}}$  position as follows:

$$\sigma_{u_{ijk}}^2 = \frac{1}{T} \int_{t-T}^t (U(\tau) - \bar{U})_{ijk}^2 d\tau \quad (4)$$

where the mean wind component is

$$\bar{U}_{ijk} = \frac{1}{T} \int_{t-T}^t U_{ijk}(\tau) d\tau \quad (5)$$

Similar expressions can be derived for the lateral and vertical turbulence component intensities  $\sigma_v$  and  $\sigma_w$ . From the standard deviations the turbulent kinetic energy can be computed as in Eq.(2).

### 4.3 Turbulent scale length

#### 4.3.1 Dryden turbulence model scale length

The filter time constants  $T_{u,v,w}$  used in the low-pass filter to filter the high-frequency turbulent white noise are computed from turbulent scale lengths as follows

$$T_{u,v,w} \equiv \frac{L_{u,v,w}}{V_{ref}} = \frac{k_{u,v,w}h}{V_{ref}} \quad (6)$$

Here  $L_u$ ,  $L_v$  and  $L_w$  are the characteristic turbulent scale lengths of the turbulence components.

For the (local, i.e. temporal) reference speed  $V_{ref}$  the sum of groundspeed  $V_{heli}(t)$  and windspeed  $V_{wind}$  is taken, assuming that for a frozen turbulence field this is the speed with which the aircraft traverses the field. Since the speeds given here are always positive, the denominator will never become negative. Flying “with the wind”, where in fact  $V_{heli} = -V_{wind}$ , cannot occur. To prevent division by zero (in case of no wind, hovering flight, in which case there is no turbulence either!) a minimum value of 5 Kt in the denominator is assumed i.e.

$$V_{ref}(t) = \text{Max}[(V_{heli}(t) + V_{wind}), 5] \quad (7)$$

The longitudinal, lateral and vertical scale lengths  $L_u$ ,  $L_v$  and  $L_w$  scale with height above ground  $h$  by the factor  $k_{u,v,w}$ . According to military references (Refs. [11] and [12]), the turbulence scale lengths at low altitudes are as

MIL-F-8785C	MIL-HDBK-1797
$L_w = h$	$2L_w = h$
$L_u = L_v = \frac{h}{(0.177 + 0.000823h)^{1.2}}$	$L_u = 2L_v = \frac{h}{(0.177 + 0.000823h)^{1.2}}$

given in Table 1.

More information can be found in Ref. [9]. With the VUmc building height being in the order of 40 m this is roughly the value of  $L_u$ ,  $L_v$  and  $L_w$ . Because of the time-varying nature of  $V_{heli}(t)$  also the time constants  $T_{u,v,w}(t)$  are time-varying.

#### 4.3.2 RANS wind model turbulent scale length

In case of the RANS wind model used to compute the flow, the turbulent scale length  $\ell$ , which defines the characteristic wave length of the turbulence variations, is obtained from a  $k-\epsilon$  turbulence model as follows (see Ref.[13]):

$$\ell = C_\mu^{3/4} \frac{k^{3/2}}{\epsilon} \quad (8)$$

where, see Refs. [9], [13],  $C_\mu = 0.09$ . Note that the scale length is the same for the  $x$ ,  $y$  and  $z$  direction, just as  $k$  and  $\epsilon$  are. With the use of the  $k-\omega$  EARS M turbulence model this coefficient  $C_\mu$  has in fact been computed as function of the grid position, see Figure 11.

As one can see (for this one slice of the data),

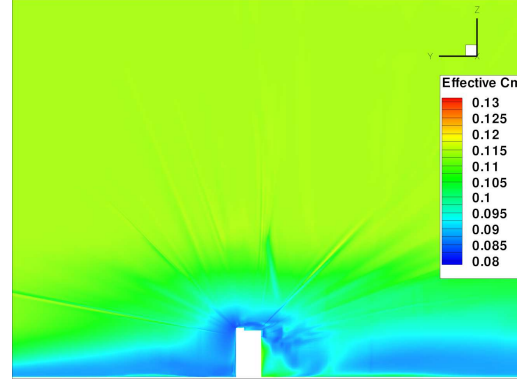


**Figure 11** Variation of  $C_\mu$  over the grid for the VUmc building

close to the building the average values seem to be indeed in the neighbourhood of 0.09, but “up and away” it tends to increase to about 0.11.

As Eq. (8) shows, in order to compute the

turbulent scale length one needs to know both the turbulent kinetic energy  $k$  and the eddy dissipation rate  $\epsilon$ . This latter parameter is derived from the computed *specific* dissipation rate  $\omega$  of the  $k-\omega$  EARS M turbulence model (see Ref. [14]) as follows:

$$\omega = C_\mu^{-1/4} \frac{\sqrt{k}}{\ell} \quad (9)$$

Substituting  $\ell$  from Eq.(8) then yields:

$$\omega = \frac{\epsilon}{C_\mu k} \Rightarrow \epsilon = C_\mu \omega k \quad (10)$$

The parameters  $k$  and  $\omega$  have been determined for the entire grid of the building and the environment over which the airflow has been computed, i.e. they vary spatially over the domain of interest. This implies that the

turbulent scale length also varies as function of  $x$ ,  $y$  and  $z$  (or  $i$ ,  $j$  and  $k$ ).

The turbulent scale *length* translates into a *time* parameter by using the same (time-varying) reference speed  $V_{ref}$  as used in Eq.(7). So the characteristic time length or period  $T$  then becomes

$$T_{ijk}(t) \equiv \frac{\ell_{ijk}}{V_{ref}(t)} = C^{3/4} \frac{k_{ijk}^{3/2}}{\mu_{ijk} \epsilon_{ijk} V_{ref}(t)} \quad (11)$$

Since the kinetic energy and eddy dissipation rate apply for each  $ijk^{\text{th}}$  grid cell in the CFD domain, the time constant depends now on the  $(x, y, z)$  position of the rotorcraft relative to the building/object, for which the CFD solution has been obtained, as well as on the time-varying speed. To prevent  $T$  from becoming too small (by  $\ell$  becoming too small), i.e. the turbulence has become white noise, a lower limit value of 0.01 has been set on  $T_{ijk}$ .

#### 4.3.3 RANS-LES wind model turbulent scale length

With the hybrid RANS-LES flow solver no specific data is generated that can be used to determine the turbulent scale length, other than determining the spectral characteristics of the variable wind components per grid point, which is inhibitive. It is therefore assumed, when working with this wind model, that the turbulent scale lengths can be determined using the variances in the wind components, coupled with the eddy dissipation rate  $\epsilon$  as obtained with the RANS solver. That is, the turbulence filter time constants are computed from

$$\begin{aligned} T_{ijk}(t) &\equiv \frac{\ell_{ijk}}{V_{ref}(t)} \\ &= C^{3/4} \frac{(\frac{1}{2}(\sigma_u^2 + \sigma_v^2 + \sigma_w^2)_{ijk})^{3/2}}{\mu_{ijk} \epsilon_{ijk} V_{ref}(t)} \end{aligned} \quad (12)$$

The above implies that for a RANS-LES model one also has to compute the RANS solver flow quantities in order to obtain  $\epsilon$ . There exists a method, the so-called “velocity method”, to compute the eddy dissipation rate from the vertical wind time history, see Refs. [15] and [16], among others. Due to lack of time this method has not (yet) been checked for its validity in applying it here, or for implementation.

## 5 REAL-TIME SIMULATIONS

### 5.1 *FlightLab model of EC135 (like)*

For the real-time simulation the rotorcraft simulation tool FLIGHTLAB™ was used. An approximate model of the EC135 helicopter was implemented, including a dual turboshaft engines drive, for which a scaled-down version of the T700 was used. The vehicle’s forces and moments are computed per blade element for each so-called Aerodynamic Computation Point “ACP” as well as for ACPs of other rotorcraft components (e.g. tail rotor, fuselage). Loads per ACP are summed over all ACPs of the simulated vehicle.



**Figure 12 Lifeliner-1 on the heli deck’s movable platform, just before the hangar**

The mean wind and turbulence data generated by the CFD solver are stored in data tables, which are input into the FLIGHTLAB model. The real-time mean winds are computed using linear interpolation in the data tables depending upon the position of each ACP, which makes the simulation calculational process very fast. The impact of the large number of stored data points is only noticeable in the time needed to load the model, but in the real-time calculation of the motion under influence of wind and turbulence the effect is minimal.

### 5.2 *Turbulence model implementation*

In the implementation in the FlightLab simulation model the aerodynamic velocity vector for a particular aerodynamic computation point “ACP” consists of the (vectorial) sum of inertial, wind and turbulence components. The inertial velocities are calculated from the simulation, the wind vector is taken from the CFD-grid data as function of  $[x, y, z]$  of each ACP, and the same is done for the turbulence components. In this way rolling, pitching or yawing gust components will likely be generated, in addition to the effect of spatial

gradients in the mean wind flow that may also contribute to angular motion upsets.

To be able to perform the test matrix (see para. 6.1) a switch has been built in the flight simulation model to switch the turbulence on or off prior to each run.

### 5.3 Visual model of the VU building

For a real-life photo of the heli deck of the Life-liner see Figure 12.

A visual object of the medical complex was provided, to be used in the visual scenery of the simulator. No other objects were available, such as other high-rise buildings in the vicinity of the VUmc building.

### 5.4 Description of the simulator

As means to evaluate the wind “climate” above the heli deck of the VUmc using piloted simulations, NLR’s fixed-base Helicopter Pilot Station “HPS” was used. It has been upgraded in 2009 with a much expanded visual system, providing a 70° vertical x 180° horizontal field of view. Four image projectors project the visual scenery onto a vertical semi-cylindrical wall. For an impression from the cockpit, looking at the VUmc, see Figure 13.



**Figure 13 Action photo of the VUmc building taken during a simulation run**

The simulator features a single set of helicopter pilot controls (right side only) and a digital control loading system produced by MOOG. All instrument layouts are shown on programmable EFIS displays. Using an internal NLR’s instrument display design tool called “Vincent” existing instrument layouts can be modified or new layouts can be quickly implemented.

## 6 SIMULATION EVALUATION

### 6.1 Goals and test plan

The goals and objectives listed were two-fold, viz.

- 1) for the pilot:
  - a) to approach and land on the heli platform on top of the VUmc-building as accurately as possible, following normal procedures. This will be done for 2 wind directions, viz. 225° (the most dominant wind direction) and 360°.
- 2) for the experiment:
  - a) to determine if there are differences in flying and handling performance, in terms of pilot workload, flight path accuracy, turbulence encountered of the rotorcraft, etc., between the two wind conditions and the 2 mean wind models (i.e. RANS or hybrid RANS-LES).
  - b) A second goal was to see if the presence or not of a turbulence model, or its type (i.e. Dryden or RANS), would affect the workload and turbulence ratings of the pilots (i.e. they might misconstrue the mean wind variations within the grid as turbulence).

The experimental design was a so-called 2 (wind direction: 225°, 360°) x 2 (wind model: RANS, RANS-LES) x 3 (turbulence filter: Dryden, RANS, none) repeated measures design. The sequence of the 2 x 2 x 3 = 12 runs per pilot was randomized across pilots so as to alleviate, if not evenly distribute, learning effects as much as possible.

Four pilots from the ANWB participated. All of them have been operating from the VUmc for at least several years.

### 6.2 Simulation execution & results analysis

The simulation set-up was evaluated using several (4) pilots from the MAA medical service, who were quite pleased with the simulation set-up.

The data gathered were both subjective and objective in nature. Subjective data are data obtained from questionnaires, while objective data were “flight” data obtained from the simulation model.

### 6.2.1 Subjective data evaluation

The main parameters questioned were 1) the

The scales were administered to the pilot after each run. After the experimentation a post-

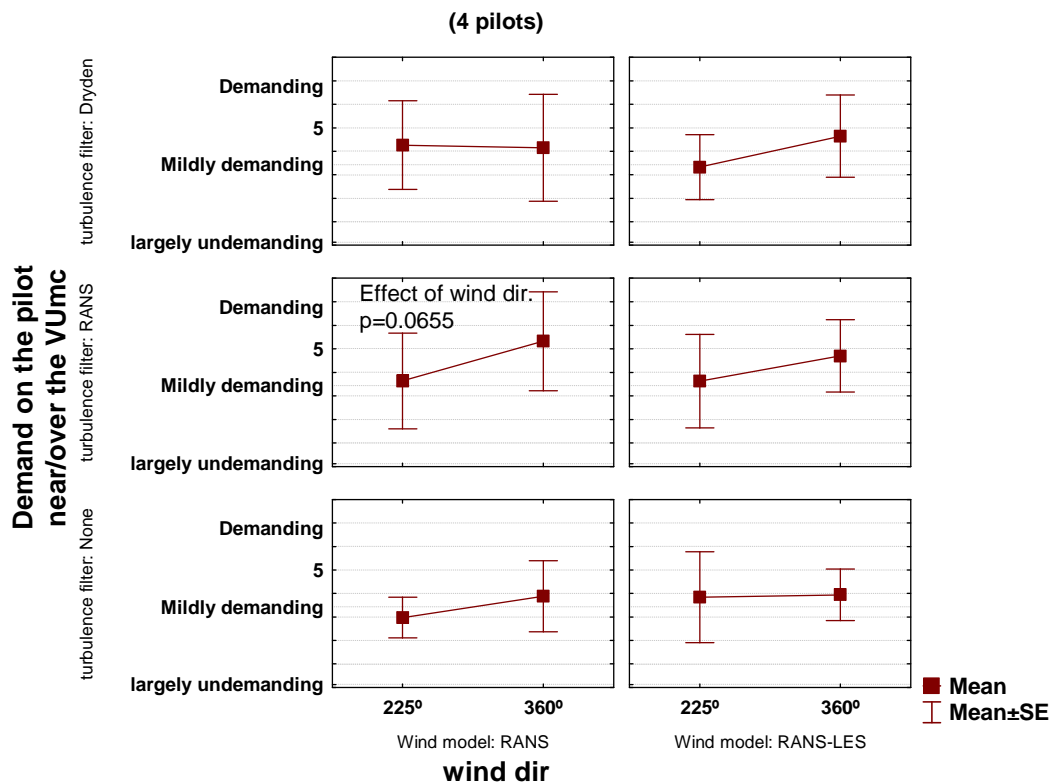


Figure 14 Mean values of “demand on the pilot” per wind dir., wind model and turbulence filter

pilot workload, 2) realism of the wind climate and 3) the turbulence intensity “experienced”. For the workload the “Demand-on-the-pilot” adjectival scale, developed in Ref. [17] was used. This scale was demonstrated to be an interval scale. NLR has quite some experience with this scale as it was found to be easy to administer, unambiguous and also quite homogeneous, in that across many pilots no biases were detected (Ref. [18]). Other workload rating scales that could have been used are the Bedford workload scale and the NASA-TLX scale. The first one is in fact an ordinal scale, much like the well-known Cooper-Harper rating scale, while the NASA-TLX are essentially 6 free scales to rate items such as temporal load, frustration level, performance, etc. These 6 scales, which should also be pre-weighted using a special sorting process, were found to be too complex to administer.

exercise questionnaire was also given to the pilot to rate overall quality of the simulation, for example, and to provide a pairwise comparison of turbulence intensity experienced as well as workload.

In the sections to follow the subjective data mentioned will be examined as function of the experimental factors listed in section 6.1 (i.e. ‘wind model,’ ‘turbulence model type’ and ‘wind direction’).

#### 6.2.1.1 Pilot workload

The run-to-run pilot workload data was analyzed using the 2 (wind direction) x 2 (wind model) x 3 (turbulence model type) repeated measures ANOVA. Mean values of the pilot’s workload for the part near/over the flight deck are shown in Figure 14, broken down per category of wind direction, wind model and turbulence filter.

The ANOVA showed none of the experimental factors to have a significant main effect on the pilot workload, nor did any of the interactions have a significant effect, except the 3-way interaction of wind model x wind direction x turbulence filter ( $F(2, 4)=11.567, p=.0217$ ). Further probing revealed that this was because only in case of the RANS wind model with the RANS turbulence filter the wind direction had a near-significant ( $p<0.05$ ) effect on the pilot workload near/over the VUmc building ( $F(1,3)=8.079, p=0.0655$ ), see Figure 14. The workload in case of wind  $360^\circ$  was more (close to “demanding”) than in case of a wind from  $225^\circ$  (“mildly demanding”). It was expected that for all combinations of filters and wind models there would be a difference in workload between the two wind directions, and although the trend is there for the RANS-LES wind model, the effect of wind direction did not have a significant effect ( $p>0.1$ ) on pilot workload.

**6.2.1.2 Realism of wind climate**

With each run the pilots were asked how realistic they thought the wind climate was. A histogram of the ratings is shown in Figure 16,

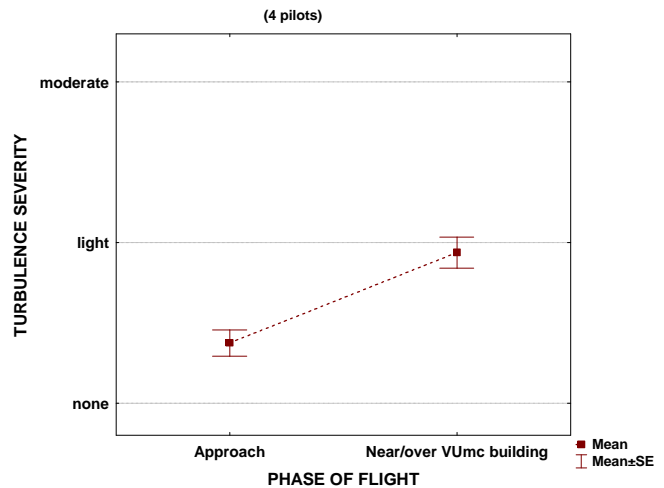


**Figure 15 Turbulence severity rating for approach and near/over the VUmc building**

vertical wind changes as they were supposed to exist, but at a (slightly) different position.

Overall the effect of wind model on rated realism was not significant (Wilcoxon matched pairs,  $Z=0.533, p=0.594$ , i.e.  $p>0.1$ ), in a statistical sense, although the RANS-LES wind model is the only wind model with, for every

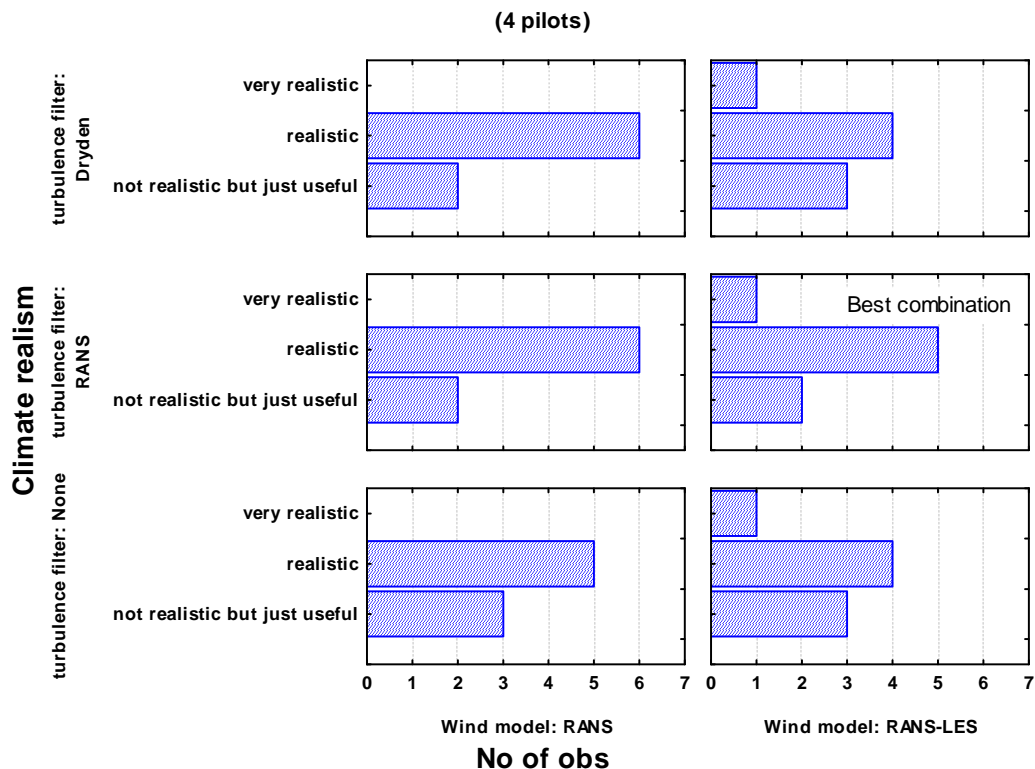


**Figure 16 Realism ratings histogram per category of wind model and turbulence filter**

broken down per wind model and turbulence filter.

One pilot rated the realism for the case of  $360^\circ$  less realistic because he ‘felt’ the headwind and

turbulence filter type, at least one score of “very realistic”. That’s why the RANS-LES wind model is favoured over the RANS model.

The “average” level, or modal response, of realism was ‘realistic’. Considering the

complexity of the modelling of the airflow around such an object this is a good result.

One major reason why pilots rated the wind modelling less realistic was there was not enough turbulence experienced farther away from the building, e.g. on the approach to the building.

### 6.2.1.3 Rated turbulence severity

Pilots were asked to rate the turbulence severity, and distinguish between 1) the overall level, 2) the approach phase and 3) the phase of flight “near or over the VUmc building”.

Both the Sign test ( $Z=3.878$ ,  $p=0.000105$ ) as well as the Wilcoxon matched pairs test ( $Z=3.629$ ,  $p=0.000285$ ) indicated that there was a highly significant ( $p<0.01$ ) difference, in a statistical sense, in rated turbulence severity between the approach phase of flight and the phase of flight near and over the building (subjectively distinguished), see Figure 15. This is not a surprise: closer to the platform there is more turbulence than farther away.

In fact one of the pilots reported there was too little disturbance, or turbulence, farther away compared to reality, for which reason he rated the realism in one case as “not realistic but useful”, see also the previous section. In an earlier experiment (Ref. [19]) it was tried to

increase this turbulence reality by adding atmospheric turbulence according to the Dryden turbulence model. The two pilots who then participated both found this ‘added’ turbulence too much for the 225° wind direction case (which was then the only wind direction tested).

Since it is hypothesized that the turbulence severity rating for the part near or over the VUmc building will correlate best with the turbulence modelled around the building, the values of this rating for near or over the VUmc building are shown in Figure 17.

The effect of wind direction on rated turbulence looks significant only for the RANS wind model with the RANS turbulence filter. The Wilcoxon’s matched pairs test showed the effect to be weakly significant ( $p<0.1$ ) at the most, viz.  $Z=1.603$ ,  $p=0.1088$ . It was already reported by some pilots before the experiment that wind from the north would be more difficult to handle than from the southwest. For the other categories of wind model and turbulence filter the wind direction did not have a statistically significant effect. So the turbulence level experience around the building in this case was fairly independent of the wind direction.

As to the effect of turbulence filter the Friedman ANOVA on ranks test gave  $\chi^2(N=12,$

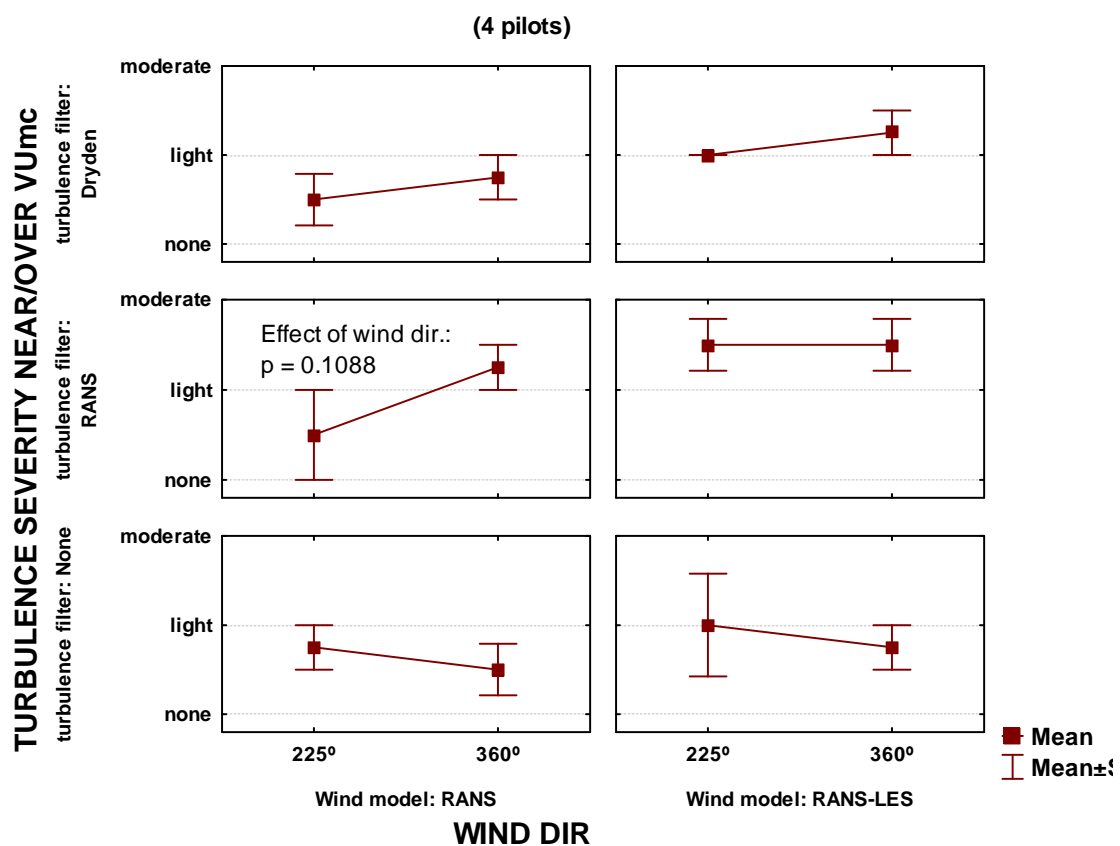


Figure 17 Turbulence severity ratings near/over the platform per wind dir., wind model and turbulence filter category

$df=2$ )=1.931,  $p = .3808$ , so the effect of the type of filter is not significant ( $p>0.1$ ). This means, for example, that the pilots could not distinguish between the RANS or Dryden filter or no turbulence at all, i.e. they rated the mean wind changes that came with the wind model as turbulence, which was expected. The wind changes are non-random deterministic variations, i.e. the same wind appears always at the same position, however, the pilots did not spend long enough time in this wind field close to the building, and due to their own flight path variability they did not pass through exactly the same position, so the wind variations experienced as turbulence were induced a) by the wind gradients due to variation in the mean air flow and due to changes in position.

It must be noted though that pilots flew towards the heli deck usually above the worst part of the turbulence field, following even a steep slope of sometimes up to  $10^\circ$  (see §6.2.2.3). They may have unknowingly avoided the worst part of the turbulence in this way. Therefore their severity ratings will not always reflect the turbulence intensity existing around the building.

All pilots rated the turbulence experienced during the experiment as “well acceptable” for both daylight and night-time operations off the heli deck.

## 6.2.2 Objective data evaluation

### 6.2.2.1 General

For objective data the parameters registered for analysis were:

- flight path ( $x, y, z$ )
- air velocities ( $U, V, W$ )
- inertial velocities ( $\dot{x}, \dot{y}, \dot{z}$ )
- attitudes ( $\theta, \phi, \psi$ ) and attitude rates ( $p, q, r$ )
- pilot control inputs (lat. cyclic, long. cyclic, collective, pedal)
- etc.

Since the flight path contains decelerations, i.e. speed changes, the time histories of the above-mentioned parameters will be manipulated to remove trends due to the speed change, or the part of the time history that correlates with speed can be removed. For example, a variable  $x$  will be modified into  $x_{mod}$  as follows:

$$x_{mod}(t) = x(t) - [aV(t) + b]$$

where  $V$  is the indicated airspeed and the coefficients  $a$  and  $b$  are determined from a regression analysis. This will make  $x_{mod}$  uncorrelated with speed  $V$ .

After removal of any linear trend with either time or distance the rms (root of the mean of the sum of squares, i.e.  $rms = \sqrt{\frac{1}{N} \sum_{i=1}^N x_i^2}$ ) has been

calculated of the parameters listed earlier, categorized into rms values for the ‘*approach*’ and the ‘*near or above the VUmc building*’ segment using a distance criterion of 1000 ft. The flight segment before 1000 ft away from the platform is the approach, closer than 1000 ft is the “*near and over the VUmc building*”. This separation criterion was found after inspection of the many flight data runs.

In the analysis that follows the pilot control activity and flight path deviation will be examined as function of the experimental factors listed in section 6.1.

### 6.2.2.2 Pilot control activities

A typical effect of correcting the control input for speed changes is shown in Figure 18.

Especially near the end, i.e. from 80 s into the flight the activity increases.

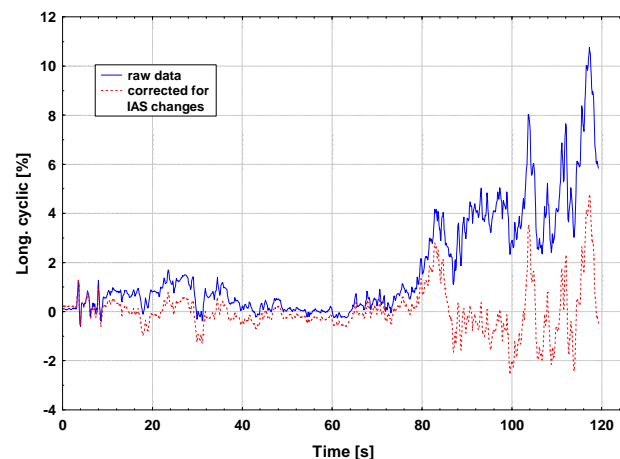


**Figure 18 Typical longitudinal cyclic with and without speed correction**

From an ANOVA on all control rms values it turned out that only wind direction and the wind model had some effect. A summary of significance of main effects of the experimental factors on the controls is given in Table 2.

As the table shows, the wind model did not have any significant effect on control activity, except in combination with wind direction (i.e. a significant interaction), see the last column. The effect of wind direction was for the collective and lateral cyclic to increase in activity for the  $360^\circ$  compared to the  $225^\circ$ . The wind model  $x$  wind direction interaction is shown in Figure 19.

**Table 2 Significance of (main) effects on control RMS**

control	WIND DIR	WIND MODEL	TURB. FILTER	FL SEGM.	INTERACTIONS
Lat. cyclic	0.018746	NS	NS	0.005854	WIND DIR x WIND MODEL (0.031992)
Long. cyclic	NS	NS	NS	0.020511	NS
Collective	0.027499	NS	NS	0.083601	WIND DIR x WIND MODEL (0.015128)
Pedal	NS	NS	NS	0.033171	WIND DIR x WIND MODEL (0.004927)

NS: Non-Significant

The significant interaction shows that the effect of wind direction on the collective and lateral cyclic is stronger than for the longitudinal cyclic and the pedal activity. Overall, though, the rms activity varied from 1 % to 4 %. The effect of wind model on the controls was non-significant.

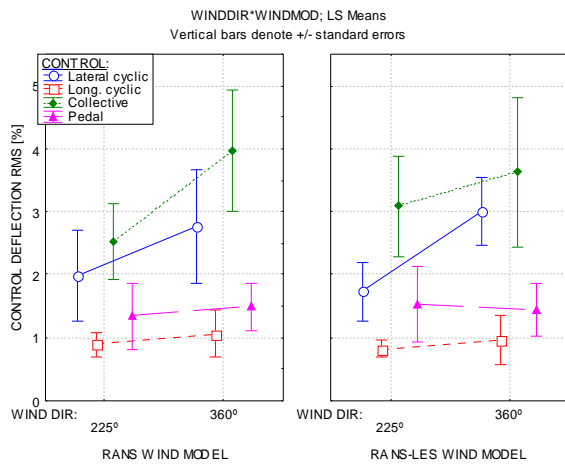


**Figure 19 Wind model x wind direction interaction effect on control rms**

The flight segment more or less obviously had a significant effect on all control

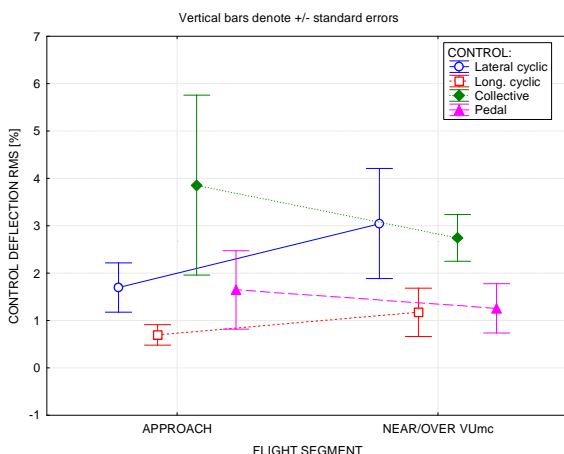


**Figure 20 Control rms per flight segment**

activities, albeit that near/over the VUmc the control activity in collective or pedal was less than in the approach, while for the lateral and longitudinal cyclic it was the opposite, which

was the expected trend. The difference in trend is shown in Figure 20.

The control activity for the collective and pedal diminished for flight near/over the VUmc because a) collective and pedal are correlated due to power changes, and the approach is the phase where the greatest power changes were made due to deceleration, while close to the building the collective had already reached higher levels because of the slow flight at that time. Overall, though, the effects of the experimental factors showed no surprising trends.

**6.2.2.3 Flight path deviations**

Concerning flight path profiles and deviations pilots were set up on a descending flight path, at a glideslope of 4.5° that would bring them right over the landing platform.

A typical altitude profile is shown in Figure 21. Rather than having followed the linear path (see the green-dotted line), as was the outset, using visual cues all pilots tended to follow a curved

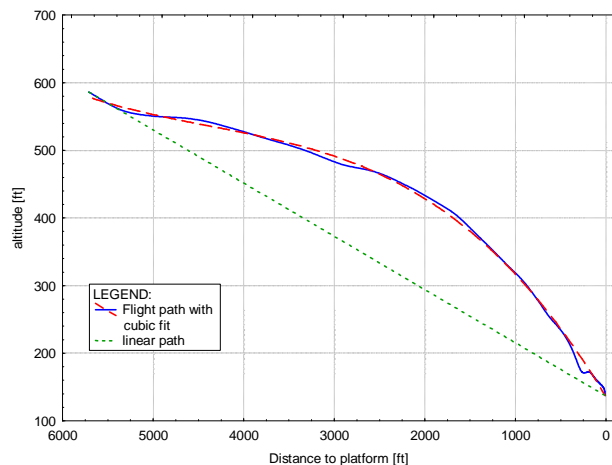


**Figure 21 Typical altitude profile, with cubic fit**

path, first by flattening the approach and then steepening the glide slope as they got closer to the platform, with the glide path angle increasing, in the case above, from 4.5° to 12.5°. In this way the aircraft would stay well above any patch of turbulence generated by the VUmc building. Because of the curve upwards first and then downwards, a very good approximation

could be made of the altitude profile using a cubic fit, see the fitted dashed red line. Therefore in the analysis of statistical variables the deviation from the curve fit, dz3, has been computed and further analyzed, since apparently this was the “normal” pilot’s behaviour.

Analysis of the variance in dz3 showed that none of the experimental factors, nor interactions between them, had any statistically significant ( $p > 0.1$ ) effect. The overall average value for the rms of dz3 was 5.2 ft, which is very small indeed. It shows how consistent the pilots were in flying the approach in their way. The cubic fit to the vertical path indicates that the flight path angle is changing (i.e. steepening) continuously, rather than being constant. This cubic fit, of the form  $z = a + bx + cx^2 + dx^3$ , can be used to easily compute the gradient of the flight path, i.e. the tangent of the flight path angle, at the helispot as  $\left. \frac{dz}{dx} \right|_{x=0} = b$ . It turned

out from an analysis of the variance that this coefficient was affected only by the wind model and the pilot who flew. The combined interaction between the two is shown in Figure 22.

The final flight path angle for the RANS-LES wind model was about 1.5° more, i.e. steeper, than for the RANS wind model. Why this was so is unknown at the moment. Especially the second pilot used quite steep flight path angles, about 4° more, than the other

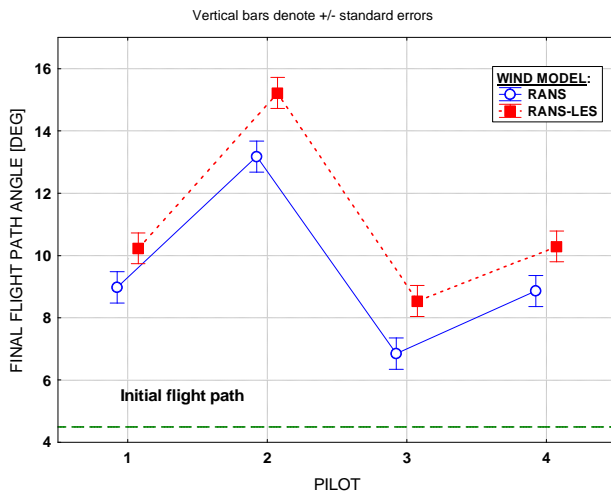


**Figure 22 Effect of wind model and pilots on final flight path angle**

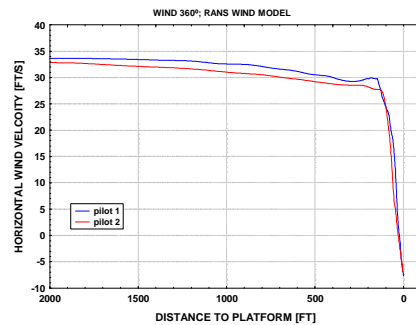
pilots, who used a more modest final flight path angle of about 10°, purely the result of visual cueing of the situation. Note that the initial flight path angle set out was 4.5°, considerably less than used by the pilots.

**6.2.2.4 Wind velocity profiles**

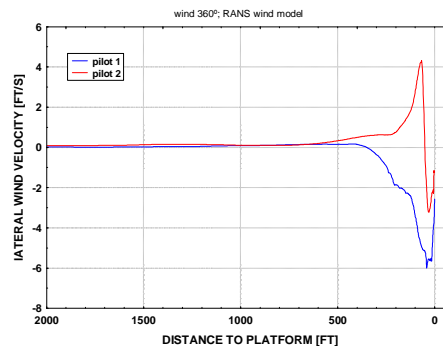
For the sake of demonstration the longitudinal, lateral and vertical wind components for the RANS wind model, with the wind coming from 360°, are shown for 2 pilots in Figure 23, parts a) through c). Pilot 2 was the one who approached the heli deck for this wind condition at an angle of about 40° from the right, i.e. he turned to the northeast first and then left to the northwest to approach the deck in order to avoid having to fly through the downwind turbulence expected to come from the building. He did this in accordance with standard practice. The other pilots did not object to approaching straight from the south. As one can see from inspecting the figure is that there is not much difference in the longitudinal wind component, the lateral wind component shows the largest difference due to the difference in approach direction, and the vertical wind component also showed difference due to the different location near the building, although in general the two wind profiles look quite similar.

These wind changes were experienced by the pilots as turbulence but, as one can see, there are no “high-frequency” variations in the wind components as is the case with the turbulent velocity profiles, see section 6.2.2.5.

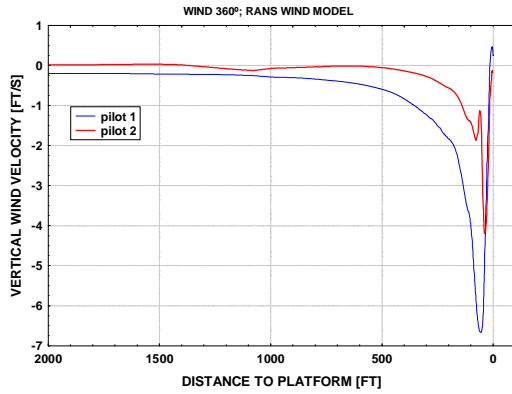
To answer the question if wind variations between the RANS and the RANS-LES wind model were different, an analysis of the variance in these wind components for the “near/over the



**a) Horizontal wind components**



**b) Lateral wind components**



c) Vertical wind components

Figure 23 Wind components for 2 pilots

building” phase of flight was performed. The ANOVA was performed on the RMS values of

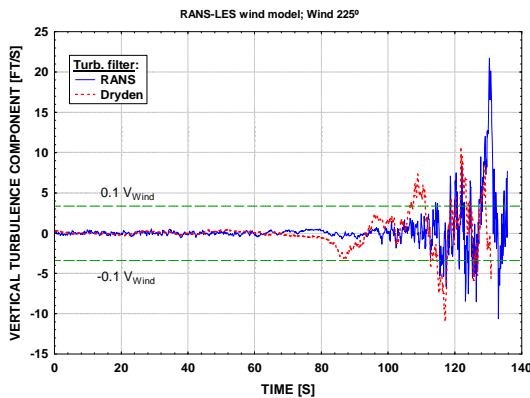


Figure 24 Vertical turbulence components (Dryden and RANS-filtered)

the vertical wind component  $RMS_z$  and on the combined RMS of the longitudinal and lateral wind component values, i.e. on  $RMS_{xy}$ , where

$$RMS_{xy} = \sqrt{RMS_x^2 + RMS_y^2} .$$

The analysis showed that the only effect present was from the wind direction, which had an almost significant ( $p < 0.05$ ) influence on  $RMS_{xy}$ ,  $F(1,2)=16.576$ ,  $p=0.0554$ . The  $RMS_{xy}$  for a wind direction of  $360^\circ$  was slightly larger, viz. 27 ft/s, than for the wind from  $225^\circ$ , viz. 26 ft/s. This, in a way, agrees with the notion made by pilots who expected the wind variations to be more severe when the wind came from the north than from the southwest. The rms in the vertical wind component was not affected at all by either wind model, wind direction or turbulence filter.

### 6.2.2.5 Turbulent velocities profile

A typical plot of the vertical turbulence component, for the two turbulence filters, is shown in case of the RANS-LES wind model, for a wind direction of  $225^\circ$  in Figure 24.

Clearly one can see the lower-frequency Dryden component as compared against the RANS-

filtered component, which shows a higher frequency content. Both components exceed the  $0.1V_{Wind}$  boundary, which is the “normal” atmospheric turbulence intensity, or sigma. It is evident from this figure also that in the early part of the approach, say before 80 seconds, the turbulence level is quite low, a remark the pilots also made.

### 6.2.3 Correlation between objective and subjective measures

Correlation coefficients were computed between the two workload ratings per run and the rms values of the flight and control activities. Results are given in Table 3. Only those correlation coefficients that could be determined with statistical significance ( $p < 0.05$ ) are included in Table 3.

From the table one may conclude that pilot workload correlated with mostly roll rate and all control activities on the (initial) approach, while near or over the VUmc the pilot workload

Table 3 Correlation between workload and other parameters

Fl. segment	parameter	workload	
		Approach	Near/over VUmc
Approach	Pitch angle	-0.327001	
	Roll rate	0.578268	0.471825
	Yaw rate	0.419341	0.383300
	Lat. cyclic	0.311266	
	Long. cyclic	0.434967	0.456027
	Collective	0.371810	
	Pedal	0.520882	0.292541
near/over VUmc	Wind x-comp	-0.290087	
	Wind y-comp	-0.404260	-0.423831
	Pitch angle	0.576798	0.632914
	Roll rate		0.312643
	Pitch rate		0.414025
	Yaw rate	0.365004	0.461039
	Lat. cyclic	0.451627	0.382374
	Long. cyclic	0.310395	0.475366
	Collective		0.333617
Pedal	0.578595	0.427100	

correlated most with pitch attitude and roll rate changes and again all control activities. Turbulence on the initial approach as well as near or over the VUmc did not correlate, surprisingly, with pilot workload, however, x-y

wind variations did (near/over the VUmc). The reason could well be that the turbulence level overall was too low to have any effect, compared to the already changing mean wind components.

## 7 CONCLUDING REMARKS AND RECOMMENDATIONS

The approach to modelling wind + turbulence using steady-state RANS and/or hybrid RANS-LES turbulence modelling worked out well, and provided a well-to-do real-time solution to the simulation of the wind environment around a complex object.

Pilots, experienced with the wind situation at the VUmc building, rated the simulation of the wind climate as ‘realistic’ and sometimes even as ‘very realistic’, even though a fixed-base simulator was used.

All pilots tended to modify the approach path such that they levelled off more or less at first, in order to arrive at a steeper glide path angle close to the platform, approaching the deck at glide path angles of between 9° and 13°.

Although there was no significant difference in realism rating with the type of wind model, the RANS-LES wind model scored the maximum realism rating of “very realistic” several times, which did not happen with the RANS wind model. It is therefore the favourite wind model for further research or application.

The type of turbulence filter, or even the absence of turbulence, did not have any effect at all on pilot’s workload or rated turbulence severity. In fact pilots were unable to discern whether the wind changes experienced were due to spatial wind gradients of a deterministic nature or due to time-varying wind components of a random nature, derived from the turbulent kinetic energy in the air flow. From pilot comments it is evident that additional turbulence modelling for the far-field situation (i.e. the initial approach) needs to be implemented, since with the present situation the far-field turbulence intensity was rated as unrealistically low. The “velocity method” developed in Ref. [15] can be a good method to obviate the need to also run the RANS solver to obtain the eddy dissipation rate when using the RANS-LES solver.

The wind and turbulence modelling approach applied in this exercise may be very well applicable to the more demanding helicopter-ship deck operations, or for modelling the wind climate around or near oil rigs.

It may be considered worthwhile to validate or confirm the findings of pilot workload and turbulence ratings using a moving-base simulator as well.

Very close to the VUmc a new building is being erected, about as tall as the VUmc building itself, about which there are grave concerns about the effect it will have on the wind climate above the flight deck. Wind-tunnel tests already performed seem to indicate a worsening of the situation, however, no verification has yet been made with piloted simulation tests and no other means exist to transform the wind-tunnel and video data into meaningful pilot workload statistics. This could be achieved by including this new building extension in the CFD model and re-run the entire process of generating mean wind flows and turbulence data with a subsequent simulation exercise.

Further expansions envisioned are the addition of more visual objects, e.g. other high-rise buildings in the vicinity of the hospital for added realism, night-time operations using a lit deck with visual cueing for guidance, and the development of reduced-noise approach and departure procedures from the heli deck within the framework of the European Green RotorCraft (GRC) Joint Technical Undertaking (JTU).

## 8 ACKNOWLEDGEMENTS

The author would like to acknowledge the highly valuable contributions given by the MAA pilots who participated in the simulation exercise, and the expert contribution in the CFD calculations and wind data generation by Jaap van Muijden of the AVFP department of NLR.

Also the effort and work done e.g. with regard to the VUmc building geometry and EC135 modelling by Tim Jager is highly appreciated. And finally great appreciation is expressed towards Jasper van der Vorst who implemented the various CFD data into a real-time version of the FLIGHTLAB simulation model and made the simulation work as it should.

This work was partly funded by the EU-funded JTU Green rotorcraft GRC 5 project and the ALICIA project (All Condition Operations and Innovative Cockpit Infrastructure).

## 9 REFERENCES

- [1] Zwakhals, S.L.N., Kommer, G.J., Kostalova, B., 2008: “*Emergency Medical Services out of hours. Supply and demand of Mobile Medical Teams during night-*

- time in the Netherlands*” (in Dutch). RIVM report 270144001/2008, 2008.
- [2] Matesanz, A., Velázquez, A., 2000: “*EARSF finite element solver for the study of turbulent 3-D compressible separated flows*”. Computer Methods in Applied Mechanics and Engineering, Vol. 190, December 2000.
- [3] Hellsten, A., 2005: “*New Advanced  $k-\omega$  Turbulence Model for High-Lift Aerodynamics*”. AIAA Journal, Vol.43, No. 9, September 2005
- [4] McIntosh, D.H., Thom, A.S., 1969: “*Essentials of Meteorology*”. Wykeham Publication (London) Ltd, 1969.
- [5] Kok, J.C., Boerstoeel, J.W., 1996: “*A robust multi-block Navier-Stokes solver for industrial applications*”. NLR TP 96323, 1996.
- [6] Kok, J.C., 2000: “*Resolving the dependence on free-stream values for the  $k-\omega$  turbulence model*”. AIAA Journal, Vol.38, NO.7, 2000. Also NLR-TP-99295, 1999.
- [7] Kok, J.C., Spekrijse, S.P., 2000: “*Efficient and accurate implementation of the  $k-\omega$  turbulence model in the NLR multi-block Navier-Stokes system*”. Paper presented at ECCOMAS 2000, Barcelona, Spain, Sep. 2000.
- [8] Kok, J.C., Oskam, B., van der Ven, H., 2004: “*Extra-large eddy simulation of massively separated flows*”, AIAA 2004-264, 2004.
- [9] Dryden spectrum.  
<http://www.mathworks.com/help/toolbox/aeroblks/drydenwindturbulencemodelcontinuous.html>
- [10] Civil Aviation Authority Safety Regulation Group: CAA Paper 2008/03, “*Helideck Design Considerations – environmental Effects*”, CAA, Norwich, Great Britain, July 2009.
- [11] U.S. Military Handbook MIL-HDBK-1797, 19 December 1997.
- [12] U.S. Military Specification MIL-F-8785C, 5 November 1980.
- [13] Turbulence length scale. [http://www.cfd-online.com/Wiki/Turbulence\\_length\\_scale](http://www.cfd-online.com/Wiki/Turbulence_length_scale)
- [14] Turbulence free-stream boundary conditions. [http://www.cfd-online.com/Wiki/Turbulence\\_free-stream\\_boundary\\_conditions](http://www.cfd-online.com/Wiki/Turbulence_free-stream_boundary_conditions).
- [15] Cornman, L.B., Meymaris, G., Limber, M., 2004: “*An update on the FAA Aviation weather research program’s in-situ turbulence measurement and reporting system*”. 11<sup>th</sup> Conference on Aviation, Range and Aerospace Meteorology, Hyannis, American Meteorological Society, P4.3, 2004.
- [16] Haverdings, H., Chan, P.W., 2010: “*Quick Access Recorder (QAR) data analysis software for studies of windshear, turbulence and wake vortex*”. International Aerospace Engineering (IREASE), Vol.3, No.2, April 2010.
- [17] McDonnell, J.D., 1968: “*Pilot rating techniques for the estimation and evaluation of handling qualities*”. Air Force Flight Dynamics Laboratory Technical Report 68-76, 1968.
- [18] Haverdings, H., Verbeek, R.J.D., 2008: “*OPTIMAL D7.3.3-1 NLR rotorcraft-ATC integrated simulations experimental results*” OPTIMAL report WP7-NLR-078-V1.0-ED-CO.
- [19] Jager, T.S., 2010: “*Simulation of the wind model around the VUmc Hospital for HEMS helicopter operations*”. Bachelor’s thesis 3.0, Hogeschool Amsterdam, November 18<sup>th</sup>, 2010.